1-1-2018

Towards thermally stable high performance lithium-ion batteries: the combination of a phosphonium cation ionic liquid and a 3D porous molybdenum disulfide/graphene electrode

Yu Ge
University of Wollongong, yg711@uowmail.edu.au

Cristina Pozo-Gonzalo
Deakin University

Yong Zhao
University of Wollongong, yz705@uowmail.edu.au

Xiaoteng Jia
University of Wollongong, xj916@uowmail.edu.au

Robert L. Kerr
Deakin University

See next page for additional authors

Towards thermally stable high performance lithium-ion batteries: the combination of a phosphonium cation ionic liquid and a 3D porous molybdenum disulfide/graphene electrode

Abstract

We report a thermally stable high-performance lithium battery using an electrochemically synthesized three-dimensional porous molybdenum disulfide/graphene composite electrode and a phosphonium-based ionic liquid (IL) electrolyte. Benefiting from the structural merits of the chosen electrode and the thermal stability of the electrolyte, the cell coupled with a Li foil exhibits excellent rate performance and cycling capability at room temperature; and that is retained with an even better rate capability at an elevated temperature of 50 8C. This work may provide a new avenue for the development of safe and high performance lithium-ion batteries at high temperature.

Disciplines

Engineering | Physical Sciences and Mathematics

Publication Details

Ge, Y., Pozo-Gonzalo, C., Zhao, Y., Jia, X., Kerr, R., Wang, C., Howlett, P. C. & Wallace, G. G. (2018). Towards thermally stable high performance lithium-ion batteries: the combination of a phosphonium cation ionic liquid and a 3D porous molybdenum disulfide/graphene electrode. Chemical Communications, 54 (42), 5338-5341.

Authors

Yu Ge, Cristina Pozo-Gonzalo, Yong Zhao, Xiaoteng Jia, Robert L. Kerr, Caiyun Wang, Patrick Howlett, and Gordon G. Wallace

Journal Name

COMMUNICATION

Towards thermally stable high performance lithium-ion batteries: the combination of a phosphonium cation ionic liquid and a 3D porous molybdenum disulfide/graphene electrode

Received 00th January 20xx,
Accepted 00th January 20xx

DOI: 10.1039/x0xx00000x

www.rsc.org/

Yu Ge[a], Cristina Pozo-Gonzalo[b], Yong Zhao[a], Xiaoteng Jia[a], Robert Kerr[b], Caiyun Wang*[a], Patrick C. Howlett*[b], and Gordon G. Wallace[a]

We report a thermally stable high-performance lithium battery using an electrochemically synthesized three-dimensional porous molybdenum disulfide/graphene composite electrode and a phosphonium-based ionic liquid (IL) electrolyte. Benefiting from the structural merits of chosen electrode and the thermal stability of the electrolyte, the cell coupled with a Li foil exhibits excellent rate and cycling capability at room temperature; and that is retained with an even better rate capability at an elevated temperature of 50 °C. This work may provide a new avenue for the development of safe and high perfromance lithium-ion batteries at high temperature.

Lithium-ion battery (LIB) technologies with increased energy storage capabilities as well as reliability at high temperature are required to meet the needs of advanced electronics.[1-3] Safety issues have received significant attention in recent years.[4] Traditional electrolytes for LIBs are composed of volatile and flammable organic solvents containing toxic lithium hexafluorophosphate ($LiPF_6$). Room temperature ionic liquids (RTILs) have low volatility with greatly reduced flammability.[5, 6] The merits of low volatility, high ionic conductivity and excellent electrochemical stability make RTILs a promising alternative electrolyte for LIBs.[7]

RTIL electrolytes based on the bis(trifluoromethanesulfonyl)imide (TFSI) or the bis(fluorosulfonyl)imide (FSI) anions coupled with nitrogen-based cation have been well studied as electrolytes in lithium/sodium batteries demonstrating stable cycling performance.[5, 6, 8-10] The recently developed phosphonium based ionic liquids offer comparable to or even superior properties than those ammonium derivatives with regards to the properties of Li^+ transport and electrochemical windows.[11-14] For instance, the IL containing phosphonium with an alkyl ether chain demonstrated an electrochemical window of 4.1 V and a high Li^+ transport number of 0.54;[12] while that with a small alkyl phosphonium imide demonstrated a high electrochemical window of 5.7 V, a low viscosity of 18.4 mPa s, and a high conductivity of 13.8 mS cm^{-1}.[13] While these features are all highly desirable for LIBs, the use of these electrolytes in lithium-ion batteries has not been reported.

To realize the full potential of an IL electrolyte in a LIB, the electrode must be well-designed with a structure that allows complete wetting and minimizes mass transport losses arising from the higher viscosities. Traditional graphite anodes may not be suitable in this regard because of its low theoretical capacity (372 mAh g^{-1}). Molybdenum disulfide (MoS_2) has emerged as a promising anode candidate owing to its high theoretical capacity (670 mAh g^{-1}).[15, 16] Moreover, it can be easily fabricated into various nanostructured composites electrodes to achieve outstanding lithium storage performance.[17, 18] MoS_2 nanosheets vertically grown on graphene sheets by the hydrothermal method delivered a large capacity of 1077 mAh g^{-1} at 100 mA g^{-1}.[17] A free-standing macroporous film composed of chemically exfoliated MoS_2 nanosheets and graphene sheets via self-assembly offered a high capacity of 800 mAh g^{-1} at 100 mA g^{-1}.[18] Recently we developed an electrochemically synthesized molybdenum sulfide/graphene nanocomposite, which exhibited a very high capacity (over 1200 mAh g^{-1} at 100 mA g^{-1}) and excellent rate performance (1016 mAh g^{-1} at 2 A g^{-1}).[19] The lithium storage performance of these MoS_2/graphene composites in an IL has not been demonstrated.

Here we propose a combination of a small phosphonium cation IL-based electrolyte with a molybdenum sulfide-based electrode for lithium storage applications. The applied electrolyte, a mixture of trimethyl(isobutyl)phosphonium bis(fluorosulfonyl)imide ($P_{111i4}FSI$) and lithium bis(fluorosulfonyl)imide (LiFSI) has demonstrated good performance in lithium batteries with a $LiNi_{1/3}Mn_{1/3}Co_{1/3}O_2$ cathode obtaining a stable capacity of 130 mAh g^{-1} over 200 cycles at 0.25 mA cm^{-2}.[14] An electrochemically deposited

[a] ARC Centre of Excellence for Electromaterials Science, Intelligent Polymer Research Institute, AIIM Facility, University of Wollongong, NSW 2522, Australia.
[b] Institute for Frontier Materials (IFM), Deakin University, Burwood, Victoria 3125, Australia.
*E-mail: caiyun@uow.edu.au, patrick.howlett@deakin.edu.au

†Electronic Supplementary Information (ESI) available: [details of any supplementary information available should be included here]. See DOI: 10.1039/x0xx00000x

molybdenum disulfide/graphene composite with a three-dimensional porous structure was used as the electrode in this work. The assembled cells exhibited excellent energy storage capacities at room temperature, and a remarkable stability and even better rate capability at higher temperature. This work may provide a good avenue towards practical LIB applications with both high performance and reliability at high temperature.

The chemical structure of $P_{111i4}FSI$ is depicted in Fig. S1 (ESI†). The physicochemical properties of $P_{111i4}FSI$ containing various concentrations of LiFSI (0.5-3.8 mol kg^{-1}) have been well studied previously[11]. We used the IL mixture with 3.2 mol kg^{-1} LiFSI in this work because of its favorable physicochemical and Li^+ transport properties for use in a LIB: no melting and crystallization along with a very low glass transition (-72.9±0.2 °C); a reasonable ionic conductivity of 0.9±0.1 mS cm^{-1}; and a larger Li transference number (0.40±0.01) than the conventional $LiPF_6$/EC/DEC electrolyte at 25 °C (0.24±0.087).[20]

The electrochemical synthesis of 3D porous MoS_2/graphene was performed in a solution containing $(NH)_4MoS_4$, graphene oxide (GO) and KCl. Upon the applied negative potential of -1.2 V, GO nanosheets decorated with MoS_4^{2-} migrated and attached onto the stainless steel mesh (SSM) substrate, where MoS_4^{2-} was converted into MoS_2 following a reaction of $MoS_4^{2-} + 2e^- + 4H^+ \rightarrow MoS_2 + 2H_2S$.[21, 22] Meanwhile, GO was reduced at such negative potential,[23] denoting the composite as MoS_2/rGO thereafter. The random stacking of these sheets created a porous 3D structure.

Scanning electron microscopy (SEM) was applied to characterize the structures. The neat MoS_2 film was uniformly coated on the SSM (Fig. 1a) with a compact structure and a thickness of ~640 nm. As revealed by both the cross-sectional view and topographic images, the MoS_2/rGO electrode displayed a porous three-dimensional (3D) architecture created by the randomly stacked nanosheets (Fig. 1b and c). Such film-like structure showed an average thickness of ~3 µm, higher than that of the molybdenum sulfide/graphene film deposited by cyclic voltammetry (1-2 µm from 30 cycles).[19] The lateral size of the composite nanosheets was in a range of several hundred of nanometers with a typical thickness of ~72 nm. At a higher magnification, the composite sheets displayed a granular surface structure (Fig. 1d). The energy dispersive X-ray spectroscopy (EDS) results clearly showed strong Mo and S peaks for both MoS_2 and MoS_2/rGO (Fig. S2a, b, ESI†), while the C peak could only be found in the spectrum of MoS_2/rGO, evidencing the existence of graphene and formation of composite. High-resolution transmission electron microscopy (HRTEM) further evidences that rGO sheets were evenly coated by MoS_2 (Fig. 1e). At a higher magnification, a lattice spacing of 0.65 nm was shown (Fig. 1f) corresponding to the (002) crystal plane of layered MoS_2. These results clearly demonstrate that graphene nanosheets may act as the template and backbone for the growth of MoS_2.

The formation of MoS_2 was confirmed by Raman, thermo-gravimetric analysis (TGA) and X-ray photoelectron spectroscopy (XPS). Distinct peaks at 354.6, 410.1 and 458.7 cm^{-1} were observed in the Raman spectra of neat MoS_2 and MoS_2/rGO (Fig. 2a), which respectively correspond to the E^1_{2g}, A_{1g} and 2LA modes of hexagonal MoS_2 crystal,[24] confirming the existence of MoS_2. For MoS_2/rGO, the D band and G band of graphene at 1322 cm^{-1} and 1601 cm^{-1} can also be found, evidencing the formation of a composite. TGA curves also provided the evidence of the formation of composite (Fig. S3, ESI†). These two materials MoS_2 and MoS_2/rGO all displayed a major weight loss at ~400 °C, which can be attributed to the oxidation of MoS_2 to MoO_3 in air.[25] An extra weight loss at ~200 °C was observed for MoS_2/rGO, mainly related to the removal of residual oxygen-containing groups in rGO.[26]

The formation of molybdenum sulfide can be further shown by the strong Mo and S peaks in the wide XPS spectrum of MoS_2/rGO (Fig. 2b), wherein the intensity ratio of S:Mo was calculated to be 1.96, very close to the stoichiometric number of crystalline MoS_2. This ratio is lower than the 2.4 obtained

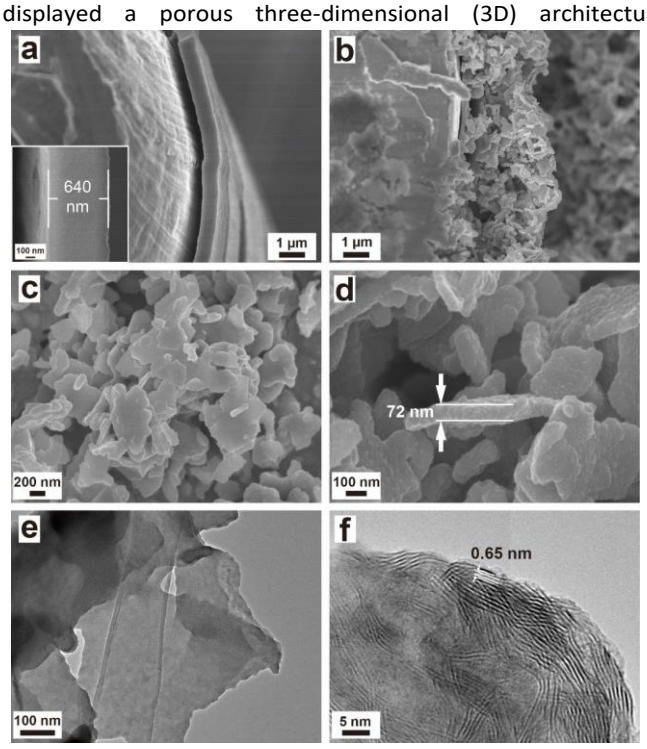

Fig. 1 SEM images of MoS_2 (a; inset shows the thickness) and MoS_2/rGO (b-d) at different magnifications; (e, f) TEM images of MoS_2/rGO.

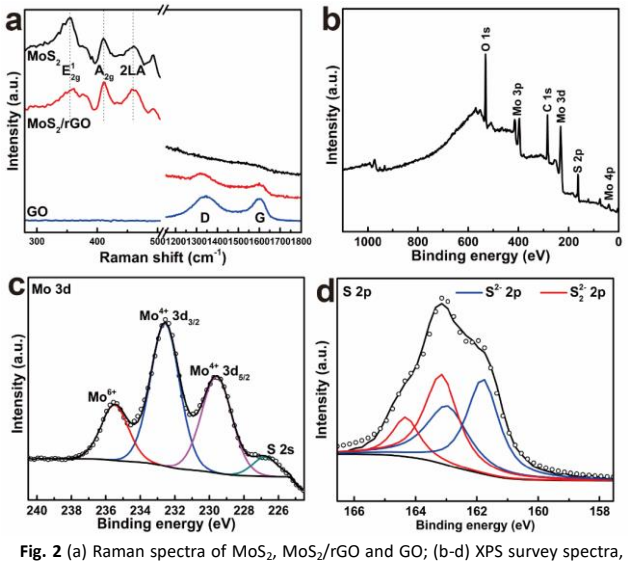

Fig. 2 (a) Raman spectra of MoS_2, MoS_2/rGO and GO; (b-d) XPS survey spectra, Mo 3d spectra and S 2p spectra of MoS_2/rGO.

for the MoS_x/rGO composite synthesized using cyclic voltammetry, since that MoS_3 was formed during the anodic process.[19] In the Mo 3d region, two major peaks at ~229.6 eV and 232.6 eV can be ascribed to Mo $3d_{5/2}$ and Mo $3d_{3/2}$ binding energies (Fig. 2c), typical for Mo^{4+} in MoS_2. The peak at ~235.5 eV is assigned to Mo^{6+}. In the S 2p region (Fig. 2d), a strong doublet at the lower binding energy (~161.8 and 163.0 eV) represent S^{2-} $2p_{3/2}$ and S^{2-} $2p_{1/2}$, characteristic S 2p peaks of MoS_2 crystals. Another weaker doublet at ~163.2 and 164.3 eV arise from S_2^{2-} $2p_{3/2}$ and S_2^{2-} $2p_{1/2}$, indicating the existence of bridging S_2^{2-} ligands, which constitutes MoS_3 in the form of $Mo^{IV}(S^{2-})(S_2^{2-})$,[27] suggesting the presence of MoS_3 of a minor content. The peaks representing C-O and C=O at ~285.2 eV and ~287.9 eV decreased dramatically in the C 1s spectra of MoS_2/rGO compared to that of GO (Fig. S4a and b, ESI†), proving the massive removal of oxygen-containing groups, namely, reduction of GO.

The electrochemical performance of the cells at room temperature was investigated using cyclic voltammetry (CV) at 0.2 mV s^{-1} and galvanostatic charge/discharge at 0.1 A g^{-1}. By referring to the mass of bare SSM substrate, the areal mass loading of the electrode was about 0.46 mg cm^{-2} for MoS_2 and 0.55 mg cm^{-2} for MoS_2/rGO. Here, four types of cells were assembled with the combination of two types of electrode (MoS_2; MoS_2/rGO labelled as MG) and two electrolytes (3.2 mol kg^{-1} LiFSI in $P_{111i4}FSI$, labelled as IL; 1 M $LiPF_6$ in 1:1 ethylene carbonate/dimethyl carbonate, labelled as CE). These cells are denoted as MG-IL, MG-CE, MoS_2-IL, and MoS_2-CE, respectively. The MG-IL cell displayed a sharp cathodic peak at ~0.5 V in the first CV cycle (Fig. 3a) corresponding to the formation of solid electrolyte interphase (SEI), a main cause for irreversible capacity in the charge/discharge profile (Fig. 3b).[17] In the following cycles, three cathodic peaks at around 1.82 V, 1.02 V and 0.41 V were shown, which can be assigned to the formation of Li_2S and Li_xMoS_2, decomposition of lithiated MoS_2, respectively.[28] In the anodic process, two major peaks at ~1.56 and 2.28 V were shown which arose from the partial oxidation of Mo forming MoS_2, and formation of sulfur, respectively.[28] In the charge/discharge profile, plateaus at ~2.0 and 1.0 V in the discharge process, and ~2.2 and 1.4 V in the charge process can be seen; they are the typical Li storage characteristics of MoS_2-based materials and are consistent with the CV results. Similar electrochemical behaviours were presented by MG-CE, MoS_2-CE and MoS_2-IL cells as well (Fig. S5, ESI†).

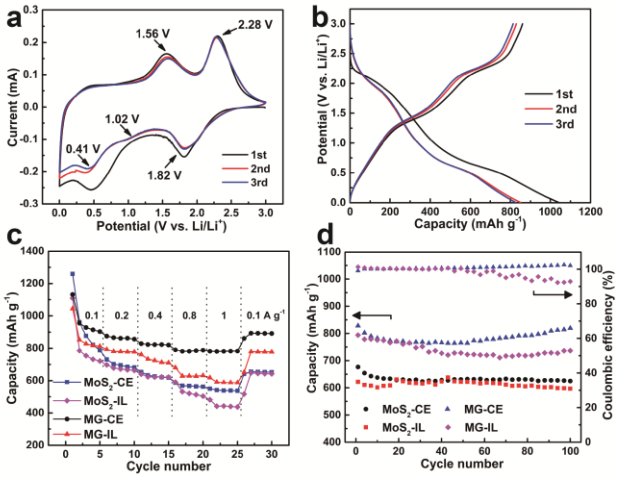

Fig. 3 (a) The first three cyclic voltammograms of the MG-IL cell over a potential range of 0.0-3.0 V vs. Li/Li+ at 0.2 mV s^{-1}; (b) The first three charge/discharge curves of MG-IL at 0.1 A g^{-1}; (c) Rate performance of the cells; (d) Cycling performance at 0.4 A g^{-1} of the cells and the Coulombic efficiency of the MG-CE and MG-IL.

The rate performance of the cells at room temperature was investigated (Fig. 3c). They all delivered a very high specific capacity of 1131, 1044, 1259 and 1109 mAh g^{-1} during the first cycle for MG-CE, MG-IL, MoS_2-CE and MoS_2-IL, respectively. The MG-CE exhibited the highest reversible capacities at all current densities investigated (0.1-1 A g^{-1}): 955, 875, 829, 790 and 782 mAh g^{-1} for 0.1, 0.2, 0.4, 0.8 and 1 A g^{-1} -applied current. The MG-IL offered a comparable capacity of 852, 793 and 761 mAh g^{-1} at a current density of 0.1, 0.2 and 0.4 A g^{-1}; a lower capacity of 629 and 590 mAh g^{-1} at 0.8 and 1 A g^{-1}. This is attributed to the higher viscosity and lower conductivity of the IL electrolyte. The rate capability of both MG cells is superior to those obtained using MoS_2, confirming advantages accrued using the 3D porous structure over that of a compact nature. It can be attributed to the following aspects: high conductivity of the rGO matrix improving the electron transport; enlarged electrolyte- electrode interface which facilitates greater Li^+ diffusion into the electrode structure. Importantly, the capacity delivered from the MG-IL cell is much higher than that of the graphite anode in FSI-based IL electrolyte (360 mAh g^{-1} at 0.2 C).[29]

The cycling performance at room temperature was studied at a current density of 0.4 A g^{-1} (Fig. 3d). All systems investigated displayed good cycling stability over 100 charge/discharge cycles, and the MG-CE showed the best cycling performance of an initial reversible capacity of 828 mAh g^{-1} and 819 mAh g^{-1} at the 100th cycle, a retention rate of 99% with a stable Coulombic efficiency close to 100%. The MG-IL delivered an initial reversible capacity of 794 mAh g^{-1} and 737 mAh g^{-1} at the 100th cycle with a retention rate of 93% and a Coulombic efficiency of 94%, which is inferior to the MG-CE cell. Nevertheless, this cycling stability is better than those of reported MoS_2/graphene composites with conventional solvent-based electrolyte, including hydrothermally synthesized composites (a retention rate of 88.6% over 100 cycles at 100 mA g^{-1})[30] and exfoliated MoS_2 nanosheets hybrid with graphene (71% retained over 100 cycles at 100 mA g^{-1}).[31]

These cells were further characterized by electrochemical impedance spectra (EIS). The Nyquist plots with a suppressed semi-circle at high-frequency region and a linear part at low-frequency region were fitted using an equivalent circuit model composed of R_s, R_{ct}, CPE and Z_W, representing contact resistance, charge transfer resistance, constant phase element, and Warburg impedance, respectively. It is noticeable that the MG-IL showed a lower R_{ct} (32 Ω) than that of the MG-CE (87 Ω)

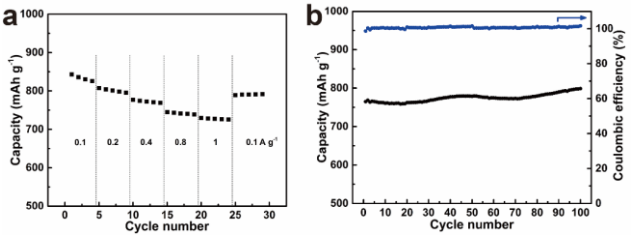

Fig. 4 Rate capability (a) and cycling performance at 0.4 A g^{-1} (b) of MG-IL recorded at 50 °C.

(Fig. S6a, ESI†). This may be attributed to the high concentration of LiFSI in the IL electrolyte, leading to an increased Li^+ transference number.[11] Both MoS_2-CE and MoS_2-IL exhibited a larger R_{ct} of 115 and 151 Ω (Fig. S6b, ESI†), which we expect is due to their compact film structure.

The charge/discharge performance of MG-IL at a high temperature (50 °C) was investigated with the MG-CE cells as controls. However, most of the MG-CE cells failed even at the first cycle, and no sufficient results could be collected. This may be ascribed to the poor thermal stability of organic solvent and the possible decomposition of $LiPF_6$ salt at 50 °C. In contrast, the MG-IL cell displayed excellent rate performance (Fig. 4a), a reversible capacity of 843, 804, 774, 743 and 728 mAh g^{-1} was delivered at 0.1, 0.2, 0.4, 0.8 and 1 A g^{-1}, respectively. The capacities at lower current densities (0.1-0.4 A g^{-1}) are very close to those recorded at room temperature, yet there is a ~20% increase in the capacities delivered at 0.8 and 1 A g^{-1}. It indicates that the ionic liquid electrolyte not just withstands the high temperature owing to its outstanding thermal stability, but also benefits from the resultant lowered viscosity and improved ionic conductivity.[10] The MG-IL showed an excellent cycling performance over 100 cycles at 0.4 A g^{-1}: the capacity did not drop but slightly ascended (Fig. 4b). Also, the Coulombic efficiency was kept at ~100% for all the cycles. The slight increase of the capacity over the cycling may be due to the slow wetting of the electrode by electrolyte. All these results suggest the potential use of P_{111i4}FSI IL electrolyte in LIBs to simultaneously ensure safety and retain high performance at high temperature.

In summary, the electrodeposited MoS_2/rGO composite as an electrode exhibited high capacities, good rate capability and good cycling stability when using P_{111i4}FSI ionic liquid-based electrolyte for lithium storage. The graphene-backboned 3D architecture provided an enhanced electrode/electrolyte interface, which facilitates easy access of IL electrolyte with high viscosity. Importantly, this type of cell demonstrated an outstanding cycling and rate performance at a high temperature of 50 °C owing to the thermal properties of IL. This work may provide a solution for fabricating high-performance and safe lithium-ion batteries at high temperatures. This concept can also be expanded to other electrochemical energy storage/conversion applications that involve the utilization of electrolyte-electrode interface such as sodium ion batteries, supercapacitors and electrocatalysis.

Dedicated to Professor Jin-Pei Cheng on the occasion of his 70th birthday. Funding from the Australian Research Council Centre of Excellence Scheme (CE 140100012) is gratefully acknowledged. G.G.W. is grateful to the ARC for support under the Australian Laureate Fellowship scheme (FL110100196). The authors thank the Australian National Fabrication Facility-Materials node (ANFF) and the UOW Electron Microscopy Centre for equipment use.

Conflicts of interest

There are no conflicts to declare.

Notes and references

1 B. Scrosati, *Nature*, **2011**, 473, 448.
2 J. B. Goodenough and K.-S. Park, *J. Am. Chem. Soc.*, **2013**, 135, 1167-1176.
3 S.-K. Kim, H.J. Kim, J.-C. Lee, P.V. Braun, H.S. Park, *ACS Nano*, **2015**, 9 8569-8577.
4 J. B. Goodenough, *Acc. Chem. Res.*, **2013**, 46, 1053-1061.
5 D. R. MacFarlane, N. Tachikawa, M. Forsyth, J. M. Pringle, P. C. Howlett, G. D. Elliott, J. H. Davis, M. Watanabe, P. Simon and C. A. Angell, *Energy Environ. Sci.*, **2014**, 7, 232-250.
6 M. Armand, F. Endres, D. R. MacFarlane, H. Ohno and B. Scrosati, *Nat. Mater.*, **2009**, 8, 621-629.
7 M. Hu, X. Pang and Z. Zhou, *J. Power Sources*, **2013**, 237, 229-242.
8 H. Yoon, P. Howlett, A. Best, M. Forsyth and D. MacFarlane, *J. Electrochem. Soc.*, **2013**, 160, A1629-A1637.
9 H. Matsumoto, H. Sakaebe, K. Tatsumi, M. Kikuta, E. Ishiko and M. Kono, *J. Power Sources*, **2006**, 160, 1308-1313.
10 S. A. M. Noor, P. C. Howlett, D. R. MacFarlane and M. Forsyth, *Electrochim. Acta*, **2013**, 114, 766-771.
11 G. Girard, M. Hilder, H. Zhu, D. Nucciarone, K. Whitbread, S. Zavorine, M. Moser, M. Forsyth, D. MacFarlane and P. Howlett, *Phys. Chem. Chem. Phys.*, **2015**, 17, 8706-8713.
12 V. L. Martins, N. Sanchez-Ramirez, M. C. Ribeiro and R. M. Torresi, *Phys. Chem. Chem. Phys.*, **2015**, 17, 23041-23051.
13 M. Hilder, G. Girard, K. Whitbread, S. Zavorine, M. Moser, D. Nucciarone, M. Forsyth, D. MacFarlane and P. Howlett, *Electrochim. Acta*, **2016**, 202, 100-109.
14 M. Forsyth, G. Girard, A. Basile, M. Hilder, D. MacFarlane, F. Chen and P. Howlett, *Electrochim. Acta*, **2016**, 220, 609-617.
15 T. Stephenson, Z. Li, B. Olsen and D. Mitlin, *Energy Environ. Sci.*, 2014, **7**, 209-231.
16 Q. Mahmood, M.G. Kim, S. Yun, S.-M. Bak, X.-Q. Yang, H.S. Shin, W.S. Kim, P.V. Braun, H.S. Park, *Nano Lett.*, 15 (2015) 2269-2277.
17 Y. Teng, H. Zhao, Z. Zhang, Z. Li, Q. Xia, Y. Zhang, L. Zhao, X. Du, Z. Du, P. Lv and K. Świerczek, *ACS Nano*, **2016**, 10, 8526-8535.
18 Y. Chao, R. Jalili, Y. Ge, C. Wang, T. Zheng, K. Shu and G. G. Wallace, *Adv. Funct. Mater.*, **2017**, 22, 1700234.
19 Y. Ge, C. Wang, Y. Zhao, Y. Liu, Y. Chao, T. Zheng and G. G. Wallace, *Small*, DOI: 10.1002/smll.201703096, 1703096.
20 S. Zugmann, M. Fleischmann, M. Amereller, R. M. Gschwind, H. Wiemhöfer and H. Gores, *Electrochim. Acta*, **2011**, 56, 3926-3933.
21 E. A. Ponomarev, M. Neumann-Spallart, G. Hodes and C. Lévy-Clément, *Thin Solid Films*, **1996**, 280, 86-89.
22 A. Ambrosi and M. Pumera, *ACS Catal.*, **2016**, 6, 3985-3993.
23 M. Hilder, B. Winther-Jensen, D. Li, M. Forsyth and D. R. MacFarlane, *Phys. Chem. Chem. Phys.*, **2011**, 13, 9187-9193.
24 V. Stengl and J. Henych, *Nanoscale*, **2013**, 5, 3387-3394.
25 Y. Xia, B. Wang, X. Zhao, G. Wang, H. Wang, *Electrochim. Acta*, **2016**, 187, 55-64.
26 H. Chen, M.B. Müller, K.J. Gilmore, G.G. Wallace, D. Li, *Adv. Mater.*, **2008**, 20, 3557-3561.
27 T. Weber, J. C. Muijsers and J. W. Niemantsverdriet, *J. Phys. Chem.*, **1995**, 99, 9194-9200.
28 X. Fang, X. Yu, S. Liao, Y. Shi, Y.-S. Hu, Z. Wang, G. D. Stucky and L. Chen, *Microporous and Mesoporous Mater.*, **2012**, 151, 418-423.
29 M. Ishikawa, T. Sugimoto, M. Kikuta, E. Ishiko and M. Kono, *J. Power Sources*, **2006**, 162, 658-662.
30 Z. Wang, T. Chen, W. Chen, K. Chang, L. Ma, G. Huang, D. Chen and J. Y. Lee, *J. Mater. Chem. A*, **2013**, 1, 2202-2210.
31 X. Zhou, L.-J. Wan and Y.-G. Guo, *Chem. Commun.*, **2013**, 49, 1838-1840.

